Insight - Material Science, 2019, 2(1) doi: 10.18282/ims.v2i1.182

Original Research Article

Hydrogen Embrittlement and Diffusion of High Strength Low Alloy Steels with Different Microstructures

Cabrini Marina[1,2,3*], Lorenzi Sergio[1,2,3], Pesenti Bucella Diego[1,2,3], Pastore Tommaso[1,2,3]

[1] *University of Bergamo, Department of Engineering and Applied Sciences, Dalmine (BG), 24044, Italy*
[2] *CSGI - Research Unit of Bergamo, Dalmine (BG), 24044, Italy*
[3] *INSTM - Research Unit of Bergamo, Dalmine (BG), 24044, Italy*
**Correspondence: marina.cabrini@unibg.it*

ABSTRACT
The paper deals with the effect of microstructure on the hydrogen diffusion in traditional ferritic-pearlitic HSLA steels and new high strength steels, with tempered martensite microstructures or banded ferritic-bainitic-martensitic microstructures. Diffusivity was correlated to the hydrogen embrittlement resistance of steels, evaluated by means of slow strain rate tests.

KEYWORDS: Hydrogen embrittlement; Hydrogen diffusion; Stress Corrosion Cracking; HSLA steels

Received: Feb. 15th, 2019 **Accepted:** Mar. 21st, 2019 **Online:** Apr. 5th, 2019

1. Introduction

Carbon and micro-alloyed steels for buried and marine pipelines are generally protected from generalized corrosion by means of protective coatings and Cathodic Protection (CP). Pipelines are polarized at cathodic potentials in the range -0.8 to -1.1 V vs SCE, but very negative values could be reached on overprotected areas close to the impressed current anodes, therefore the electrochemical hydrogen evolution reaction can take place[1,2]. Adsorbed atomic hydrogen, produced on the metal surface by the cathodic reaction, can enter the metal through a diffusion process owing to its high solubility in the metal lattice, with various consequences that are generally called hydrogen damage. In the presence of a susceptible material and an adequate mechanical stress, fracture in the metal can occur due to the occurrence of Hydrogen Embrittlement (HE). Different theories have been proposed to explain the hydrogen assisted cracking mechanism[3-12].
Due to the Hydrogen Enhanced Decohesion (HEDE) - also called Hydrogen Induced Decohesion (HID) mechanism - the hydrogen accumulated at a crack tip lowers the cohesive energy of the iron lattice, giving rise to a reduced fracture toughness[6,7], which describes the brittle fractures observed in metals caused by HE. The effect of hydrogen on ductile fracture can be explained by means of the Hydrogen Enhanced Localized Plasticity (HELP) theory, for which hydrogen redistribution occurs around dislocations and reduces the elastic interaction energy between them; consequently, the shear stress necessary to move the dislocations decreases and material softening arises[8]. The model of Hydrogen Enhanced Strain-Induced Vacancies (HESIV) proposes that the primary function of hydrogen in degradation is to enhance the strain-induced creation and agglomeration of vacancies, thus promoting an easy formation and linking of microvoids for the fracture process[9,13]. HE susceptibility of steels increases with their mechanical properties[14-16].

Traditional HSLA steels are produced by means of hot rolling or controlled rolling and have ferrite-pearlite banded microstructures, oriented along the rolling direction, with a different ferrite grain dimension. Quenched and tempered steels are also used with microstructures varying from martensite to acicular ferrite depending on the tempering temperature, as well as carbides. On the other hand, given the increased pressure of the transported oil/gas and the decreased wall thickness of the pipes[17], there has been a trend towards the increase in the relevant mechanical properties of pipeline steels, particularly as the use of high-strength steel pipelines is cost effective. In recent years, API 5L X100 grade steel has been developed and installed in recently constructed pipelines in northern Canada and the Japanese Sub-Sea[18-20].

Over the last few years the International Standards on CP have been modified to introduce critical values of negative potentials that cannot be exceeded in case high strength steels are used. The ISO 15589-1:2015 standard specifies that the CP potential of high strength steels (yield strength above 500 MPa) and corrosion-resistant alloys - such as martensitic and duplex stainless steels - shall be determined correctly in order to avoid the risk of hydrogen formation on the metal surface.

HE risks, either microbiologically produced or due to CP, have also been considered in the ISO 19902:2007 standard in which it is specified that HE susceptibility increases with the yield strength for steels with a specified minimum yield strength (SMYS) values in the range of 460-500 MPa. However, field experience has demonstrated that thermo-mechanically controlled processed steels with SMYS values between 450 and 480 MPa are not susceptible to HE[21].

In the field, the observation of HE is mainly associated with the presence of hard spots[22]. The critical role of the hard spots can be ascribed to the presence of martensite which is the most susceptible microstructure to HE[11,23-25]. Furthermore, Razzini *et al* -by visualizing the hydrogen distribution in an artificial hard spot on API 5L X60 steel with the use of a photoelectrochemical technique - demonstrated that the solubility of hydrogen in the heat affected zones of hard spots is higher than in the base material[26].

In the absence of microstructural alterations few cases were observed, and only in buried pipelines subject to slow plastic deformations[27-29] or mechanical damage and landslides[30]. Corrosion-Fatigue (CF) can occur on sea lines as a result of the combined action of cyclic stress and corrosive environment[21,31-33]. In this regard, there are numerous laboratory studies reported by different authors on HE on pipeline steels[1,34-43]. Nevertheless, some aspects of this phenomenon remain poorly understood.

The DNV recommended practice (DNV-RP-B401) also discusses many details relating to the protection potential of high strength steel and suggests laboratory tests to evaluate the risk of HE that can occur under CP. For instance, constant extension rate testing (SSR) is applicable to compare the susceptibility of steels from the same class (i.e. hot rolled) but a comparison between different classes is not applicable. In HE, hydrogen must be continuously supplied at the crack tip for propagation, thus the crack growth rate was controlled by the hydrogen transport rate, the applied stress and the steel intrinsic susceptibility.

This study reports the influence of microstructure on hydrogen diffusivity in HSLA steels for pipelines. Hydrogen electrochemical permeation tests were presented as a function of direction with respect to the rolling direction in order to evaluate the effect of anisotropy. The diffusivities are correlated to the hydrogen embrittlement susceptibility evaluated by means of slow strain rate tests. The results are compared to literature data and previous results[21,44-48].

2. Materials and methods

The tests were carried out on three ferrite-perlite API 5L X65 steels for off-shore pipelines (**Table 1** and **Table 2**). The steels show microstructures oriented along the rolling direction (**Figure 1**). Steel A and B were produced by means of hot rolling. Steel C was produced by means of controlled rolling.

Hydrogen permeation tests were carried out according to the electrochemical methods proposed by Devanathan-Stachurski[49]. A metal membrane was settled in a permeation cell between two compartments and acted as a bielectrode. One side (hydrogen entry side) was in contact with a NaCl 0.6 M solution and polarized at -1050 or -1500 mV vs SCE by means of a potentiostat and a platinum counter electrode. The opposite side (hydrogen exit side) was in contact with a 0.1M NaOH solution and polarized at +200 mV vs. SCE. The reference electrode was a double junction Saturated Calomel Electrode (SCE). The electrode surface was 1 cm^2 wide. The temperature was regulated at 25 °C with a thermostat. The solution in the cathodic compartment (hydrogen entry side) was re-circulated in order to avoid concentration variations and formation of hydrogen bubbles on the metal membrane. The anodic current on hydrogen exit side was monitored during the permeation test until a steady state of the hydrogen permeation flux was reached[50]. The diffusion coefficient (D_{eff}) was evaluated along the three principal directions: rolling direction, perpendicular to transverse section (T), transverse direction, across thickness, perpendicular to rolling surface (P) and transverse direction perpendicular to the longitudinal section (L) using the time-lag method[51]. Some tests were carried out on specimens with the anodic side electroplated with palladium.

Slow Strain Rate (SSR) tests were performed on 3 mm diameter cylindrical tensile specimens at strain rates ranging from 10^{-3} to 10^{-7} s^{-1} in aerated substitute ocean water (ASTM D1141-75 Standard Specification) under cathodic protection. The test solution flowed from a 25-liter reservoir, by means of a membrane pump, into a 200 mL cell made of glass and PTFE. CP was applied with a potentiostat by using a saturated calomel electrode (SCE) as reference and graphite as counter electrode.

The hydrogen embrittlement effects were evaluated by normalizing the Reduction in Area (RA) to the value obtained after the test in air. Fracture analysis was also performed in order to establish brittle areas on the fracture surface and secondary cracks.

Table 1. Chemical composition

Steel	C	Mn	Si	P	S	Cr	Ni	Mo	Nb	Cu
X65 A	0.09	1.64	0.24	0.003	0.002	0.031	0.017	0.002	0.049	0.011
X65 B	0.08	1.60	0.31	0.009	0.003	0.053	0.034	0.006	0.046	0.043
X65 C	0.05	1.55	0.16	0.002	0.003	0.031	0.005	0.248	0.041	0.015

Table 2. Producing processing, microstructure and mechanical properties

Steel	Production processing	Microstructure	TYS (MPa) $R_{p,0.2\ Long}$	UTS (MPa)	Ferrite grain size (μm)		
					Longitudinal section[1]	Transverse section	Planar section
X65 A	Hot rolling	Ferrite-pearlite	399	518	15	16	25
X65 B	Hot rolling	Ferrite-pearlite	485	567	19.5	20	16
X65 C	Controlled rolling	Ferrite-pearlite	507	579	11	9.4	10

[1] Longitudinal section perpendicular to rolled section

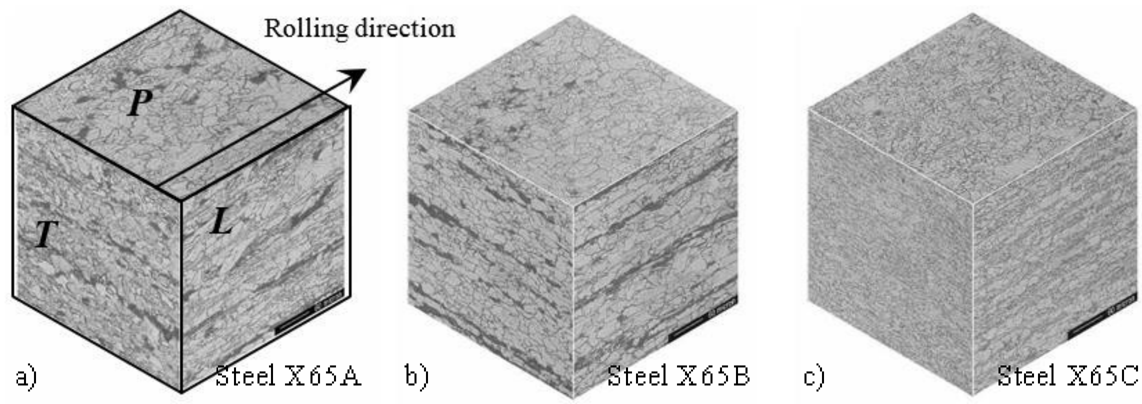

Figure 1. Microstructure of the X65 steels

3. Results and discussion

Figure 2 shows the permeation curves measured across the longitudinal section, which is the circumferential direction of the pipe. The passivity current was subtracted from the permeation curves. **Table 3** reports the values of D_{eff}. The hydrogen diffusion coefficients are independent from the potentials and there is a fairly good reproducibility between the tests with and without the palladium coating. Steel X65C has hydrogen diffusion coefficients higher than the other steels. There is no evidence of anisotropy of the hydrogen diffusion coefficients related to the rolling direction. Probably the thickness of the specimens is too high, if compared to the grain dimension, to allow the evaluation of any difference between the diffusivity in the different directions.

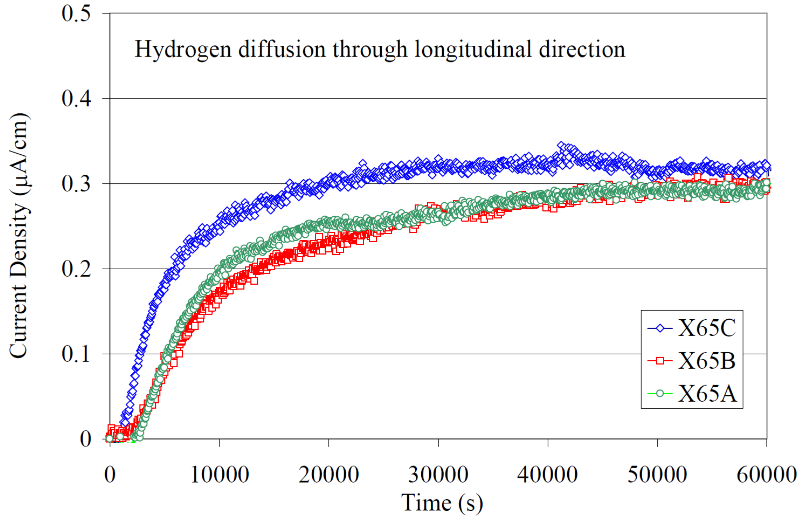

Figure 2. Example of permeation curves

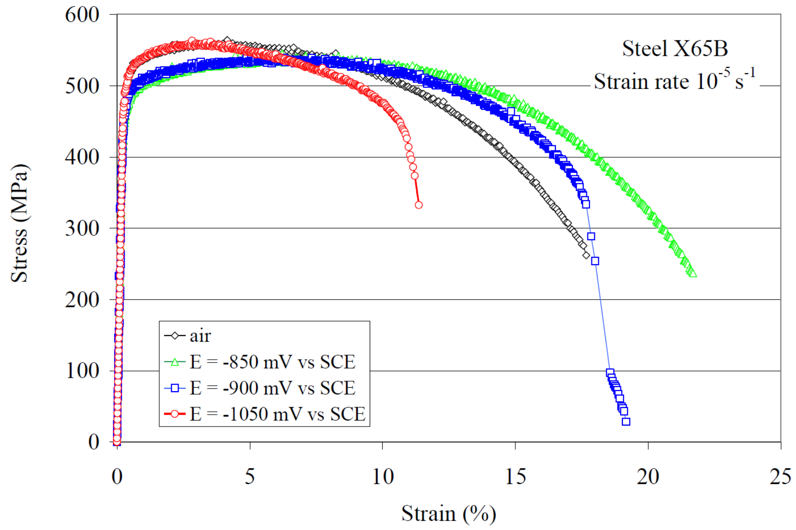

Figure 3. Stress vs strain curves obtained in the SSR tests on the specimens of X65B steel in artificial sea water under cathodic protection at strain rate 10^{-5} s^{-1} and different applied potential.

Table 3. Results of the permeation tests. E= -1050 mV vs SCE

Steel	X65A			X65B			X65C		
	P	T	L	P	T	L	P	T	L
$D_{eff} \times 10^7$ (cm^2/s)	2.6	0.9 1.9[1]	2.0 2.0[1]	2.7 2.2 1.7 3.6[2]	2.2 2.0[1]	1.4 2.0[1]	4.2 3.0[2]	4.4 4.1[1]	4.6 3.1[1]

[1] anodic side electrochemically coated with palladium; [2] Test at E = -1500 mV vs SCE

Table 4. Hydrogen diffusion coefficients of similar steels reported in literature

Steel	X60[1]		X60[1] quenched	X80[2]	X100[1]		X65M[2]	X85M[2]
Section	P	T	P	P	P	T	P	P
$D_{eff} \times 10^7$(cm^2/s)	5.6 11.5	8.5	3.7	4.7	3.9	3.9	4.2	4.0

[1]Data by Cabrini *et al.* [45] [2]Data by Zucchi *et al.* [48]

Table 5. Microstructure, mechanical properties and chemical composition of steels in **Table 4**

Steel	Production processing	Microstructure	TYS (MPa)	UTS (MPa)	C	Mn	Si	P	S	Cr	Ni
X60	Hot rolling	Ferrite/pearlite	430[2]	588	0.22	1.35	0.24	0.012	0.024	<0.01	0.01
X80	Controlled rolling and accelerated cooling	Ferrite/pearlite /bainite	547[2]	658	0.07	1.89	0.19	0.017	0.006	n.d.	0.28
X100		Ferrite/martensite	663[2]	750	0.07	1.96	0.34	0.035	0.007	0.03	0.31
X65M	Oil quenching and tempering	Tempered martensite	552[2]	619	0.10	1.12	0.30	0.010	0.002	0.142	0.418
X85M			637[3]	738	0.10	1.11	0.29	0.015	0.002	0.17	0.42

[1](% weight); [2]$R_{p,0.2\ Long}$; [3]$R_{T,0.5\ Long.}$

Table 6. Results of the SSR tests in artificial sea water or ([1]) NaCl 35 g/L solution

Steel	Strain rate								
	10^{-4} (s^{-1})			10^{-5} (s^{-1})			10^{-6} (s^{-1})		
E (V vs SCE)	-0.90	-0.95	-1.05	-0.80	-0.85	-0.90	-0.95	-1.05	-0.85
X60 [5]	1[1]	1[1]	0.7[1]		1[1]	1[1]		0.5[1]	0.95
X65A	1	0.8			0.8	0.7		0.7	0.7
X65B	1	0.7			1	0.8		0.6	0.5
X65C	0.9	0.5			0.9	0.7		0.6	0.4
X80 [5]	1			1	0.9	1[1]; 0.9	0.8	0.6[1]	0.9
X100 [5]	1[1]	1[1]	0.9[1]	1[1]	1[1]	1[1]	0.9[1]	0.7[1]	0.9
X65M [5]	1[1]	1[1]			1[1]	1[1]		0.7[1]	0.9
X85M [5]	0.7	1		1	0.9	1[1]; 0.9	0.7	0.9[1]	0.9

Table 4 summarises the D_{eff} values measured on steels that were studied in previous researches[45,48]. **Table 5** shows their chemical composition and microstructures. They were obtained by means of controlled rolling and accelerated cooling (steels X80 and X100) or by quenching and tempering (steel X65M and X85M). The first two steels have a banded microstructure of very fine ferrite and present martensite and bainite inside the ferrite bands. The quenched and tempered steels have a microstructure of tempered martensite, with small rounded carbides uniformly distributed at the acicular ferrite grain boundaries. The diffusivities in X80, X65M and X80M steels were measured by Zucchi *et al*.[48]. In **Table 4** the D_{eff} values measured on a X60 steel produced in the „60s by means of hot rolling are also reported. This steel is characterized by a coarse micro-structure of ferrite and pearlite and present several manganese sulfur inclusions, oriented along the hot rolling direction. The old X60 steel has the highest diffusion coefficients. After quenching, this steel showed a diffusivity similar to that of the martensitic steels (**Table 4**)[45]. The X100 steel has a hydrogen diffusion coefficient very close to that of the martensitic steels, while the X80 steel has an intermediate value of D_{eff}. Some authors suggested that the dominant transportation path of hydrogen in the banded ferrite/pearlite steels is along the ferrite grain boundaries and the ferrite/pearlite interfaces[52]. Luu and Wu demonstrated by means of a microprint technique that in ferritic/pearlitic steels the main hydrogen paths are represented by grain interior (lattice) and carbide-ferrite interface. For the same authors, in mar- tensitic steels the main diffusion paths of hydrogen are lath interfaces[53].

The three X65 steels considered in this paper showed similar stress vs strain curves in SSR tests carried out in artificial sea water, at 10^{-5} s^{-1} (**Figure 3**). The hydrogen embrittlement effects become evident only at potentials more negative than - 1000 V vs SCE. The examination of the fracture surface shows the presence of secondary cracks and brittle areas on the necking zone on the specimens tested at potentials lower than -850 mV vs SCE. The RA of the specimens decreases at very negative cathodic potentials, due to more evident hydrogen effects (**Table 6**).

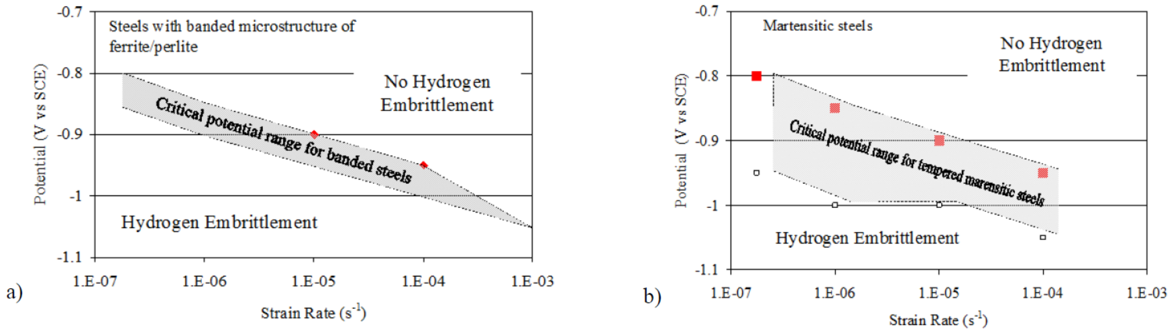

Figure 4. Effect of strain rate on critical potentials for hydrogen embrittlement

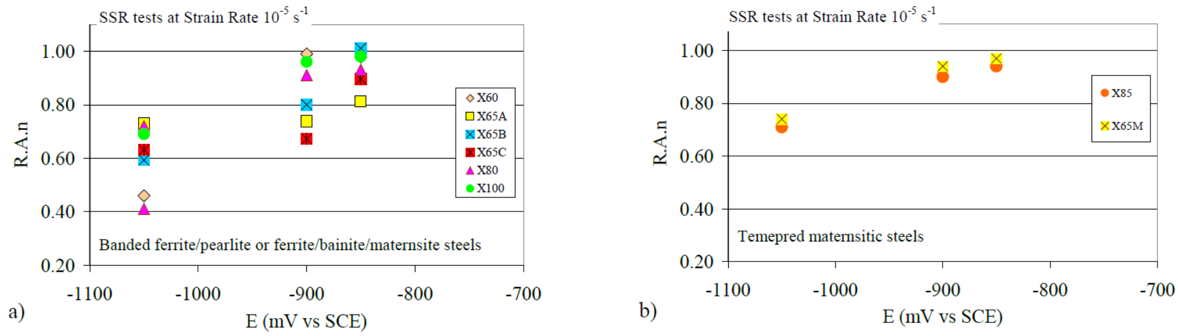

Figure 5. Normalised reduction of area after SSR tests in synthetic sea water under cathodic protection at 10^{-5} s^{-1} strain rate vs applied potential

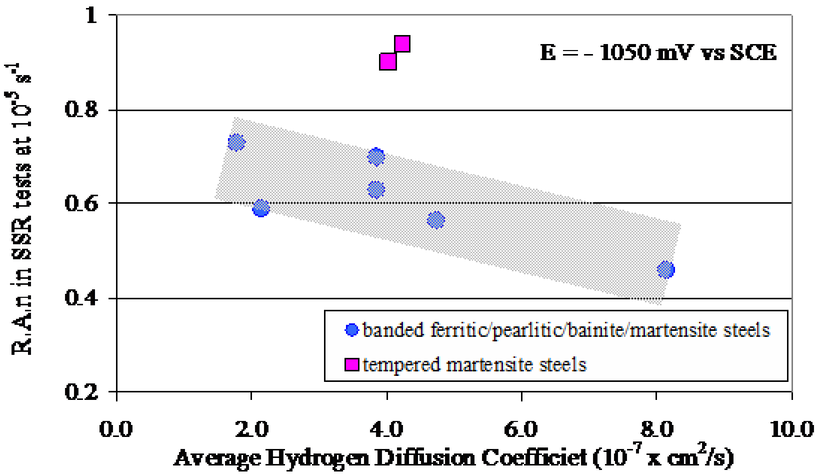

Figure 6. Normalized reduction of area in SSR tests in sea water under cathodic protection at strain rate 10^{-5} s^{-1} as a function of the average hydrogen diffusion coefficient

The examination of the fracture surface of the specimens was used in order to identify the critical value of potential for HE; value which is a function of strain rate. The steels with banded microstructures of ferrite/pearlite or ferrite/pearlite/bainite/martensite showed similar critical potentials, within a range of 50 mV (**Figure 4a**). Instead, martensitic steels showed spread values, with differences of about 150 mV (**Figure 4b**). This critical potential is related to the cracking initiation, and especially to the adsorbed hydrogen concentration, but not to the hydrogen diffusion coefficient into the steel. The differences evidenced by the martensitic steels were attributed to their heat treatment, especially to the size and distribution of carbides in their microstructure[21,54].

Figure 5 reports the normalized RA as a function of the potential during the SSR tests at strain rate 10^{-5} s^{-1}. Values less than 1 are due to the hydrogen phenomena occurring in the specimen. It is evident that the differences between the behavior of the different steels become clearly visible at -1050 mV vs SCE.

In **Figure 6** the values of the normalized RA are related to the average hydrogen diffusion coefficient. For the banded steels, it is possible to individuate an increase in the hydrogen embrittlement phenomena as the hydrogen diffusion coefficient increases. Thus, the crack propagation, evaluated by means of the normalized RA, can be related to the efficiency of the hydrogen transport. Therefore, the evaluation of the hydrogen diffusion coefficient could be useful in order to implement a fast and economic method to evaluate the potential susceptibility to HE of newly developed low alloy steels and to qualify welding procedures.

4. Conclusions

The hydrogen diffusion coefficients and the hydrogen embrittlement resistance of the examined pipeline steels depend on microstructure. A correlation between the average diffusion coefficient and the SSR results was found for the rolling banded microstructure steels. The quenched and high-temperature tempered steel, with a sorbitic microstructure, showed the highest resistance to HE.

Acknowledgements

Special thanks to Paolo Marcassoli for his help in the experimental work.

References

1. Shipilov, A. S.; May, I. L. Structural integrity of aging buried pipelines having cathodic protection. Engineering Failure Analysis, 2006; 13: 1159-76. https://doi.org/10.1016/j.engfailanal.2005.07.008
2. Shipilov, S. A. Critical assessment of the rule of cathodic protection in pipeline integrity and reliability. In: AL., F. P. E. Engineering structural integrity assessment: need and provision. Sheffield: EMAS, 2002. p. 155-62.
3. Beachem, C. D. A New Model for Hydrogen-Assisted Cracking (Hydrogen Embrittlement). Metallurgical Transactions 1972; 3: 437-51. https://doi.org/10.1007/BF02642048
4. Bernstein, M.; Thompson, A. W. Effect of Metallurgical Variables on Environmental Fracture. International Metal Review 1976; 21; 269-87.
5. Lynch, S. P. Mechanisms of Hydrogen Assisted Cracking - A review. In: MOODY, N. R., *et al*. Hydrogen effects on Materials Behavior and Corrosion Deformation Interactions. [S.l.]: TMS (The Miner- als, Metals and Materials Society) 2003; 1; 449-66.
6. Troiano, A. R. The role of hydrogen and other interstitials in the mechanical behaviour of metals. In: Trans. ASM 52 1960; 54-80.
7. Oriani, R. A. Mechanicistic Theory of Hydrogen Embrittlement of Steels. Berichte Der Bunsen-Gesellschaft Fur Physikalische Chemie 1972; 76, (8) 848-57.
8. Ayas, C.; Deshpande, V. S.; Fleck, N. A. A fracture criterion for the notch strength of high strength steels in the presence of hydrogen. Journal of the Mechanics and Physics of Solids 2014; 63, 80-93. DOI: 10.1016/j.jmps.2013.10.002
9. Nagumo, M. Hydrogen related failure of steels - a new aspect. Materials Science and Technology 2004; 20 (8) 940-50. https://doi.org/10.1179/026708304225019687
10. Srinivasan, R.; Neeraj, T. Hydrogen Embrittlement of Ferritic Steels: Deformation and Failure Mechanisms and Challenges in the Oil and Gas Industry. JOM 2014; 66 (8) 1377-82. DOI:10.1007/s11837-014-1054-4
11. Hirth, J. P. Effects of Hydrogen on the Properties of Iron and Steel. Metallurgical Transactions A 1980; 11a; 861-90. https://doi.org/10.1007/BF02654700
12. Wallaert, E. *et al*. TDS Evaluation of the Hydrogen Trapping Capacity of NbC Precipitates. In: Somerday, B. P.; Sofronis, P. International Hydrogen Conference (IHC 2012): Hydrogen-Materials Interactions 2014; Chapter 62.
13. Cabrini, M.; Lorenzi, S. Pipeline Steels: Hydrogen Diffusion and Environmentally Assisted Cracking. In: Encyclopedia of Iron, Steel, and Their Alloys (a cura di): George E. Totten Rafael Colas. [S.l.]: Tay- lor and Francis, 2016. p. 2547-2599.
14. Hardie, D.; Charles, E. A.; Lopez, A. H., Hydrogen embrittlement of high strength pipeline steels. Corrosion Science 2006; 48 (12) 4378-85. DOI: 10.1016/j.corsci.2006.02.011
15. Sandoz, G. A unified theory for some effects of hydrogen source, alloying elements, and potential on crack growth in martensitic AISI 4340 steel. Metallurgical Transactions 1972; 3 (5); 1169-76. https://doi.org/10.1007/BF02642449
16. Farrell, K.; Quarrell, A. G. Hydrogen embrittlement of an ultra-high-tensile steel. Journal of Iron and Steel Institute 1964; 202; 1002-11.
17. Demofonti, G., Spinelli C.M., Marchesani. F., *et al*., Eni TAP Project mechanical damage and Environ- mental Assisted Cracking - Full scale methodology overview. Proc. Int. Conf. New Developments on Metallurgy and Applications of High Strength Steels. Buenos Aires, 2008.

18. Jin, T. Y.; Liu, Z. Y.; Cheng, Y. F. Effect of non-metallic inclusions on hydrogen-induced cracking of API5L X100 steel. International Journal of Hydrogen Energy 2010; 35; 8014-21. 10.1016/j.ijhydene.2010.05.089
19. Corbett, K. T.; Bowen, R. R.; Petersen, C. W. High strength steel pipeline economics. International Journal of Offshore and Polar Engineering 2004; 14; 75-79.
20. Glover, A. Et al. Design Application and Installation of an API5L X100 pipeline, 2003. Proc. of the 22nd International Conference on Offshore Mechanics and Arctic Engineering, OMAE2003. Cancun, Mexico; American Society of Mechanical Engineers. 2003. p. 37429.
21. Cabrini, M., Lorenzi, S., Pellegrini, S. *et al*. Environmentally assisted cracking and hydrogen diffusion in traditional and high-strength pipeline steels. Corrosion Reviews 2015; 33 (6); 529-45. DOI 10.1515/corrrev-2015-0051
22. Carter, C. S.; Hyatt, M. V. Review of Stress Corrosion Cracking in Low Alloy Steels with Yield Strength Below 150 ksi. In: Stress Corrosion Cracking and Hydrogen Embrittlement of Iron Base Alloys. Houston: NACE, 1977. p. 524-600.
23. Kim, J. S., Lee H.Y., Lee D.I., *et al*. Effect of inter-granular ferrite on hydrogen delayed fracture resistance of ultrahigh strength boron-added steel. ISIJ (The Iron and Steel Institute of Japan) International. 2007; 47, 913-19. https://www.phase-trans.msm.cam.ac.uk/2005/LIN K/66.pdf
24. Ham, J. O.; Kim, B. G.; Lee, S. H. Measurement method of sensitivity for hydrogen embrittlement of high strength bolts. Korean Journal of Metals and Materials 2011; 49; 1-8.
25. Arafin, M.; Szpunar, J. Effect of bainitic micro-structure on the susceptibility of pipeline steels to hydrogen induced cracking. Materials Science and Engineering A 2011; 528 (15); pp.4927-4940.
26. Razzini, G., Cabrini, M. Maffi, S. *et al*. Effect of Heat-Affected Zones on Hydrogen Permeation and Embrittlement of Low Carbon Steels. Materials Science Forum 1988, 289-292, 1257-66.
27. Ha, H.; Ai, J.; Scully, J. Effects of Prior Cold Work on Hydrogen Trapping and Diffusion in API X-70 Line Pipe Steel During Electrochemical Charging. Corrosion 2014; 70(2); pp. 166-184.
28. Punter, A.; Fikkers, A. T.; Vanstaen, G. Hydrogen-Induced Stress Corrosion Cracking on a Pipeline. Materials Performance 1992; 31; 24-28.
29. Cabrini M, Lorenzi, S. Marcassoli, P., *et al*. Effetto della diffusione dell‟idrogeno sui fenomeni di EAC di acciai per pipeline in condizioni di protezione catodica. La Metallurgia Italiana 2008; 2; 15-22.
30. Cabrini, M., Pistone, V., Sinigaglia, E., *et al*. Unique Hsc Scenario Leads to Gas Line Failure. Oil & Gas Journal 2006; 6; 61-65.
31. Fassina, P., Brunella, M., Lazzari, L., *et al*. Effect of hydrogen and low temperature on fatigue crack growth of pipeline steels," Engineering Fracture Mechanics 2013; 103; pp. 10-25.
32. Baxter, D. P.; Maddox, S. J.; Pargeter, R. J. Corrosion fatigue behavior of welded risers and pipelines. 26th International Conference on Offshore Mechanics and Arctic Engineering, OMAE 2007. San Diego, California, 2007; Paper no. 29360.
33. Hu, H.; Akid, R. A Comparison of Short Fatigue Crack Growth (SFCG) rates in a Medium Strength Steel, under in-air and Corrosion Fatigue loading conditions. In: MOODY, N. R., *et al*. Hydrogen effects on Materials Behavior and Corrosion Deformation Interactions; TMS (The Minerals, Metals and Materials Society), v. 1, 2003. 617-627.
34. Payer, J. H.; Berry, W. E.; Boyd, W. K. Constant strain rate technique for assessing stress-corrosion susceptibility. Stress corrosion - new approaches. In: ASTM STP 610. Philadelphia: ASTM; 1976. p. 82- 93.
35. Kasahara, K.; Isowaki, T.; Adachi, H. Study on hydrogen-stress cracking susceptibilities of line pipe steels. Frankfurt/Main: Dechema1; 1981; 394-399.
36. Hinton, B. R. W.; Procter, R. P. M. The effect of strain-rate and cathodic potential on the tensile ductility of X-65 pipeline steel. Corrosion Science 1983; 23 (2); 101-23. https://doi.org/10.1016/0010-938X(83)90110-5
37. Punter, A.; Fikkers, A. T.; Vanstaen, G. Hydrogen induced stress corrosion cracking of the R.A.P.L. oil transmission pipeline as a result of the combined effect of cathodic protection and plastic deformation. Proceedings of the 9th international pipe protection conference. London: Elsevier. 1991. p. 257-269.
38. Rebak, R.B., Xia, Z. Safruddin, R., *et al*. Effect of Solution Composition and Electrochemical Potential on Stress Corrosion Cracking of X-52 Pipeline Steel. Corrosion 1996; 52; 396-405. https://doi.org/10.5006/1.329212.
39. Gu, B., Yu, W. Z., Luo, J.L., *et al*. Transgranular Stress Corrosion Cracking of X-80 and X-52 Pipeline Steels in Dilute Aqueous Solution with Near-Neutral pH. Corrosion 1999; 55 (3); 312-8. https://doi.org/10.5006/1.3283993
40. Trasatti, S. P., Sivieri, E., Mazza, F. Susceptibility of a X80 steel to hydrogen, Materials and Corrosion 2005; 56 (2) 111-7. https://doi.org/10.1002/maco.200403821
41. Zielinski, A.; Domzalicki, P. Hydrogen degradation of high-strength low-alloyed steels. Journal of Materials Processing Technology 2003; 133 (1-2); 230-5. https://doi.org/10.1016/S0924-0136(02)00239-X
42. Dong, C.F., Liu, Z.Y., Li, X.G., *et al*. Effects of hydrogen-charging on the susceptibility of X100 pipeline steel to hydrogen-induced cracking. International Journal of Hydrogen Energy 2009; 34; 9879-84.
43. Bosch, C., Bayle, B., Magnin, T., *et al*. Proposal for a critical test to classify the SCC resistance of materials. In: AL., M. N. E. Hydrogen effects on material behavior and corrosion deformation interactions. Warrendale: TMS, 2003. p. 587-596.

44. Haq, A., Muzaka, K., Dunne, D., *et al*. Effect of microstructure and composition on hydrogen permeation in X70 pipeline steels. International Journal of Hydrogen Energy 2013; 38(5); pp. 2544-2556.
45. Cogliati, O.; Cabrini, M. Effetto-della microsttrutura sulla diffusione dell 'idrogeno in acciai al carbonio per pipeline. La Metallurgia Italiana 2003; 3; 13-20.
46. Cabrini, M.; Maffi, S.; Razzini, G. Evaluation of Hydrogen embrittlement behaviour by means permeation current measure in slow strain rate conditions of a micro-alloyed steel. In: Bonora, P.; Deflorian, F. Electrochemical Methods In Corrosion Research Vi Pts 1 And 2 Book. Materials Science Forum. Zurich-Uetikon:Transtec Publications LTD, v. 289-292, 1998. p. 1245-1256.
47. Cabrini, M.; Razzini, G.; Tarenzi, M. Hydrogen Permeation and Embrittlement of a Low Alloyed Steel. In: Proceedings of NACE International Conference “Corrosion in Natural and Industrial Environments: problems and solutions”. Grado (Gorizia), 1995. p. 325-333.
48. Zucchi, F., Grassi, V., Frignani, A., *et al.* Influenza degli ioni solfuro sulla permeazione di idrogeno in acciai ad alta resistenza. Atti del Convegno Nazionale AIM. Vicenza: AIM. 2004. p. CD-ROM.
49. Devanathan, M.; Stachurski, Z. The adsorption and diffusion of electrolytic hydrogen in palladium. Proc Royal Society London. Series A, Mathematical and Physical Sciences; 1962; 90-102.
50. Cabrini, M., Lorenzi, S., Pesenti Bucella, D., *et al*. Effetto del carico ciclico sulla diffusione di idrogeno in acciai basso-legati. La Metallurgia Italiana 2018; 110(10); pp. 26-31.
51. Mcbreen, J.; Nonis, L.; Beck, W. A Method for Determination of the Permeation Rate of Hydrogen Through Metal Membranes. Journal of Electrochemical Society 1966; 113 (11); 1218-22. doi: 10.1149/1.3087209
52. Tau, L., Chan, S. L. I. Effects of ferrite/pearlite alignment on the hydrogen permeation in an AISI 4130 steel. Materials Letters 1996; 29, (1-3); 143-7; https://doi.org/10.1016/S0167-577X(96)00140-1.
53. Luu, W. C.; Wu, J. K. The influence of microstructure on hydrogen transport in carbon steels. Corrosion Science 1996; 38 (2) 239-45. doi: 10.1016/0010-938X(96)00109-6
54. Cabrini, M., Lorenzi., S. Marcassoli, P., *et al*. Hydrogen embrittlement behavior of HSLA line pipe steel under cathodic protection. Corrosion Reviews 2011; 29; 261-70. DOI 10.1515/corrrev-2015-0051